Seasonal Prediction of Killing-Frost Frequency in South-Central Canada during the Cool/Overwintering-Crop Growing Season

ZHIWEI WU

Key Laboratory of Meteorological Disaster, Ministry of Education, Nanjing University of Information Science and Technology, Nanjing, Jiangsu, China, and Atmospheric Numerical Weather Prediction Research Section, Environment Canada, Dorval, Québec, Canada

HAI LIN

Atmospheric Numerical Weather Prediction Research, Environment Canada, Dorval, Québec, Canada

YUN LI

Mathematics, Informatics and Statistics, CSIRO, Perth, Western Australia, Australia

YOUMIN TANG

Environmental Science and Engineering, University of Northern British Columbia, Prince George, British Columbia, Canada

(Manuscript received 22 February 2012, in final form 19 July 2012)

ABSTRACT

Seasonal killing-frost frequency (KFF) during the cool/overwintering-crop growing season is important for the Canadian agricultural sector to prepare and respond to such extreme agrometeorological events. On the basis of observed daily surface air temperature across Canada for 1957–2007, this study found that more than 86% of the total killing-frost events occur in April–May and exhibit consistent variability over south-central Canada, the country's major agricultural region. To quantify the KFF year-to-year variations, a simple index is defined as the mean KFF of the 187 temperature stations in south-central Canada. The KFF variability is basically dominated by two components: the decadal component with a peak periodicity around 11 yr and the interannual component of 2.5–3.8 yr. A statistical method called partial least squares (PLS) regression is utilized to uncover principal sea surface temperature (SST) modes in the winter preceding the KFF anomalies. It is found that most of the leading SST modes resemble patterns of El Niño–Southern Oscillation (ENSO) and/or the Pacific decadal oscillation (PDO). This indicates that ENSO and the PDO might be two dominant factors for the KFF variability. From a 41-yr training period (1957–97), a PLS seasonal prediction model is established, and 1-month-lead real-time forecasts are performed for the validation period of 1998–2007. A promising skill level is obtained. For the KFF variability, the prediction skill of the PLS model is comparable to or even better than the newly developed Canadian Seasonal to Interannual Prediction System (CanSIPS), which is a state-of-the-art global coupled dynamical system.

1. Introduction

Killing-frost events are one of the major agrometeorological disasters during the crop-growing season in Canada (e.g., Zhang et al. 2000; Shabbar and Bonsal 2003; Vincent and Mekis 2006; Qian et al. 2010). Frequent occurrences of killing-frost events often lead to reduced production in agriculture. Therefore, seasonal prediction of killing-frost frequency (KFF) is of critical importance for the agricultural sector to identify risks and opportunities, and prepare for such extreme agrometeorological events. However, extensive research into this area has yet to be conducted. This motivated us to carry out the present work and we will focus on

Corresponding author address: Prof. Zhiwei Wu, Key Laboratory of Meteorological Disaster, Ministry of Education, Nanjing University of Information Science and Technology, Nanjing, Jiangsu 210044, China.
E-mail: wzw.lasg@gmail.com

DOI: 10.1175/JAMC-D-12-059.1

the cool/overwintering-crop growing season (April–September). Cool/overwintering crops include, among others, wheat, barley, canola, oat, rye, strawberry, alfalfa, timothy, apple, pear, peach, cherry, plum, grape, and chestnut.

According to the definition of Qian et al. (2010), KFF during the cool/overwintering-crop growing season refers to the number of days with minimum surface air temperature (Ts) below −2°C from April through September. Seasonal prediction of KFF is a challenging issue, because killing-frost events are usually on synoptic time scales and a synoptic event may become unpredictable beyond a few days to 2 weeks (Lorenz 1965). Nevertheless, time or space averages of synoptic events, or the statistical behavior of KFF, may be predictable over time scales of seasons or longer due to interactions between the atmosphere and the more slowly varying oceans and land surface properties, such as sea surface temperature (SST) and snow cover, etc. (e.g., Namias 1959, 1965; Charney and Shukla 1981; Barnett et al. 1987; Robinson et al. 1993; Shabbar and Khandekar 1996; Shukla 1998; Wang et al. 2000; Wu et al. 2009; Wang et al. 2010; Lin and Wu 2011).

As a matter of fact, many studies have explored how to predict the seasonal mean of extreme weathers with precursory low boundary conditions. For instance, Wu et al. (2011b) used SST and snow cover in the preceding March to predict the extreme temperature conditions associated with the growing-season start of warm-season crops across Canada. Lin and Wu (2011, 2012) found that the autumn Tibetan Plateau snow cover extent may improve seasonal prediction of the extremely anomalous 2009/10 winter in North America. Zhang et al. (2011) established a forecasting scenario with SST conditions during the preceding October for the occurrence of anomalous wet and cold Januarys in southern China. Using the prior North Pacific SST and Arctic sea ice concentration, Wu et al. (2011a) developed an empirical model to predict the extreme winter conditions like 2007/08, during which persistent once-in-a-century snowstorms occurred over southeastern Asia.

The aforementioned studies may provide a sense of direction for the seasonal prediction of KFF in the major Canadian agricultural regions during the cool/overwintering-crop growing season. In this paper, we attempt to answer the following questions: What are the basic features of KFF in Canada and how do we quantify the KFF year-to-year variations over the major Canadian agricultural regions? How are the KFF variations linked to large-scale atmospheric circulations and previous SST conditions? The most important issue is how to predict the KFF variability.

This paper is organized as following. Section 2 introduces the datasets, model, and methodology used in this study. Section 3 suggests that most killing-frost events occur during April–May in Canada and exhibit a consistent variability over south-central Canada (south of 65°N). From this, a KFF index is defined as the mean KFF of the 187 temperature stations south of 65°N, which is dominated by two components: the decadal (DC) and interannual (IA) components. Section 4 presents the large-scale three-dimensional circulation features associated with the DC and IA components and identifies the associated dominant SST modes in the preceding December–February (DJF). In section 5, two partial least squares (PLS) seasonal prediction models are established to predict the DC and IA components, respectively. Real-time forecasts are performed for the period 1998–2007. The last section summarizes our major findings and discusses some outstanding issues.

2. Data, model, and methodology

The main datasets used in this study include 1) the homogenized historical daily Ts at 210 relatively evenly distributed temperature stations across Canada for the period 1957–2007 [Vincent et al. 2002; for the distribution of stations, see Fig. 1 in Wu et al. (2011b)]; 2) the 40-yr European Centre for Medium-Range Weather Forecasts (ECMWF) Re-Analysis (ERA-40; Uppala et al. 2005) and the ERA-Interim reanalysis dataset (Dee et al. 2011); 3) the SST data from the extended reconstructed SST, version 2 (ERSST V2), data (Smith and Reynolds 2004); 4) the Pacific decadal oscillation (PDO) index (http://www.esrl.noaa.gov/psd/data/correlation/pdo.data), defined as the leading principal component (PC) of monthly SST anomalies in the North Pacific Ocean; and 5) the Niño 3.4 index, which is defined as the averaged SST anomaly in 5°N–5°S, 170°–120°W.

Also used are the historical 1-month-lead forecast data of daily minimum Ts for the period of 1998–2007 coming from the hindcast experiment of the Canadian Seasonal to Interannual Prediction System (CanSIPS), which consists of two coupled atmosphere–ocean–ice–land climate models (versions 3 and 4 of the Canadian Community Atmosphere Model, CanCM3 and CanCM4, respectively) developed at Canadian Center for Climate modeling and analysis (CCCma). CanCM3 uses the CanAM3 atmospheric model (also known as AGCM3; Scinocca et al. 2008) with horizontal resolution of about 315 km (T63) and 31 vertical levels, together with the CanOM4 ocean model with horizontal resolution of about 100 km and 40 vertical levels and the Canadian Land Surface Scheme (CLASS) land model (Verseghy 2008). Sea ice dynamics are treated as a cavitating fluid, as described in Flato and Hibler (1992). CanCM4 (Arora et al. 2011) uses the atmospheric model CanAM4 (also

known as AGCM4) again with horizontal resolution of T63 but with 35 vertical levels. The CanOM4 ocean, CLASS land, and cavitating fluid sea ice components are essentially the same as in CanCM3. CanSIPS has been recently implemented at Environment Canada for operational seasonal predictions. It exhibits an excellent level of skill in ENSO prediction, ranking second among the eight major seasonal forecast systems (Lee and Merryfield 2010). The hindcast, generated under the second Coupled Historical Forecast Project (CHFP2), was produced according to the guidelines of the Climate-system Historical Forecast Project (CHFP) of the World Climate Research Program (WCRP). It consists of a 10-member ensemble for each of the two CCCma models, and is initialized at the beginning of each month with a 12-month integration.

The period of our analysis on KFF covers from 1957 through 2007. To get a longer time length, the ERA-40 and ERA-Interim data are combined together. We use the ERA-40 data for the period 1957–2002 and extend the data from 2003 through 2007 by using the ERA-Interim data. To maintain temporal homogeneity, the 2003–07 ERA-Interim data were adjusted by removing the climatological difference between the ERA-40 and ERA-Interim data [for the methods see Wang et al. (2010) and Wu et al. (2011b)].

To reveal the dominant SST patterns associated with the KFF variations, we employ the PLS regression method. Specifically, PLS regression embodies the well-known concept of partial correlation, as it seeks the predictors Z, which are linear combinations of factors X, being referred to as *latent vectors* or PLS *components*, and maximizes 1) the variance explained in Y and 2) the correlation between X and Y (Haenlein and Kaplan 2004; Smoliak et al. 2010). Unlike the empirical orthogonal function (EOF) analysis, which identifies major patterns explaining SST variations, using PLS regression we can find the PLS components of SST variations that best explain the covariance between SST variations and the KFF variations in Canada. In other word, it reveals the dominant SST patterns that not only account for most of the SST variations but are also closely related to the KFF variability in the region.

3. Major features of KFF during the cool/overwintering-crop growing season

Figure 1a presents the climatology of KFF across Canada during the cool/overwintering-crop growing season. A prominent feature is that the KFF values increase with latitude, which indicates that the cool/overwintering-season crops in high-latitude regions experience more killing-frost days than those in low-latitude regions. In addition, western Canada often sees fewer killing-frost events than does eastern Canada. Another notable feature is that killing-frost events occurring in April–May (AM) make up 86.2% of the total, while only a minor portion occur in September (Fig. 1b). Therefore, in the following sections we will focus on the AM season for seasonal prediction of the KFF.

Figure 2 exhibits the two leading EOF modes of KFF across Canada during the cool/overwintering-crop growing season for the period 1957–2007. The EOF1 mode accounts for 27.3% of the total variance (Fig. 2a). According to the rule given by North et al. (1982), the EOF1 mode is significantly distinguished from the rest of the eigenvectors in terms of the sampling error bars (not shown). The EOF2 mode accounts for 11.7% of the total variance and is also distinguished from the other modes (Fig. 2c). The agrometeorological meaning of the first two modes is examined here.

The EOF1 mode basically shows a monosign pattern with maximum loading located in northern Canada and its amplitude decreasing southward (Fig. 2a). This pattern primarily resembles that of the climatological mean (Fig. 1a) and reflects a consistent variability in the whole Canada KFF. PC1 exhibits a notable shift in phases and magnitudes around 1990: PC1 has more significant negative values before 1990 and positive values with larger magnitudes after 1990 (Fig. 2b).

The prominent feature of the EOF2 mode is a meridional dipole pattern with anomalies of opposite signs between south-central and northern Canada: a positive KFF anomaly center is located in central Canada and a negative center in northern Canada (Fig. 2c). This indicates that a high PC2 year corresponds to more killing-frost events in south-central Canada and fewer in northern Canada, and vice versa. PC2 is basically dominated by interannual variations, and its amplitude has increased considerably since 1990 (Fig. 2d).

Before investigating its seasonal prediction, we first need to examine the quantification of the KFF year-to-year variability in Canada. We propose a simple KFF index, which is defined as the mean KFF of 187 temperature stations south of 65°N. This definition is based on two facts. One is that the major Canadian agricultural regions are basically concentrated in the regions south of 65°N, since the regions north of 65°N are too cold for crop growing. The other is that KFF exhibits a consistent variability over the regions south of 65°N as far as the two leading EOF modes are concerned (Figs. 2a and 2c).

Figure 3a presents the time series of the standardized KFF index for 1957–2007 (black curve). It involves two time scales: the DC and the IA time scales (Figs. 3b and 3c). The latter is dominant, which accounts for around 79% of the total variances. Nevertheless, to reach a better

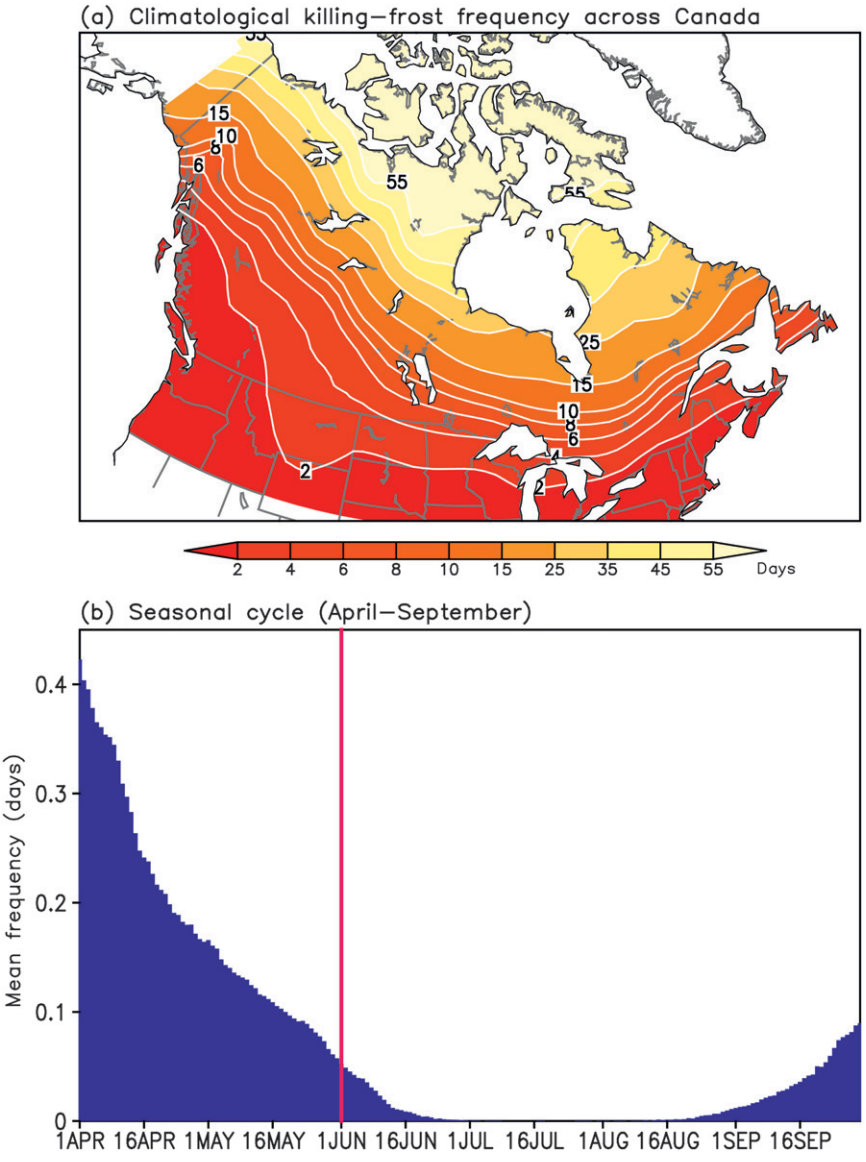

FIG. 1. (a) Climatological mean of KFF across Canada during the cool/overwintering-crop growing season (April–September) (color shadings in unit of days). (b) Seasonal cycle of the Canada mean KFF from April through September (blue bars in days). The vertical purple line indicates 1 Jun. The climatological mean and the seasonal cycle are calculated on the basis of the period 1957–2007.

level of seasonal prediction skill, we decomposed the KFF index time series into the DC and the IA components, namely, KFF(DC) and KFF(IA) (red and green curves, respectively, in Fig. 3a). The IA component contains all Fourier harmonics that have periods of less than 8 yr, while the DC component contains all Fourier harmonics that have periods longer than 8 yr, including the interdecadal variations. Figures 3b and 3c display the power spectrum of the DC and IA components. The KFF(DC) peak is centered around 11 yr, and the KFF (IA) around 2.5–3.8 yr. The latter is close to the typical periodicity of El Niño–Southern Oscillation (ENSO) (e.g., Ropelewski and Halpert 1986).

In the following section, we will identify three-dimensional circulation structures associated with the DC and IA components of the KFF variability and their predictability sources, respectively.

4. Circulation structures and predictability sources

As mentioned above, we focus on the AM season. Figure 4 shows AM surface circulation anomalies regressed

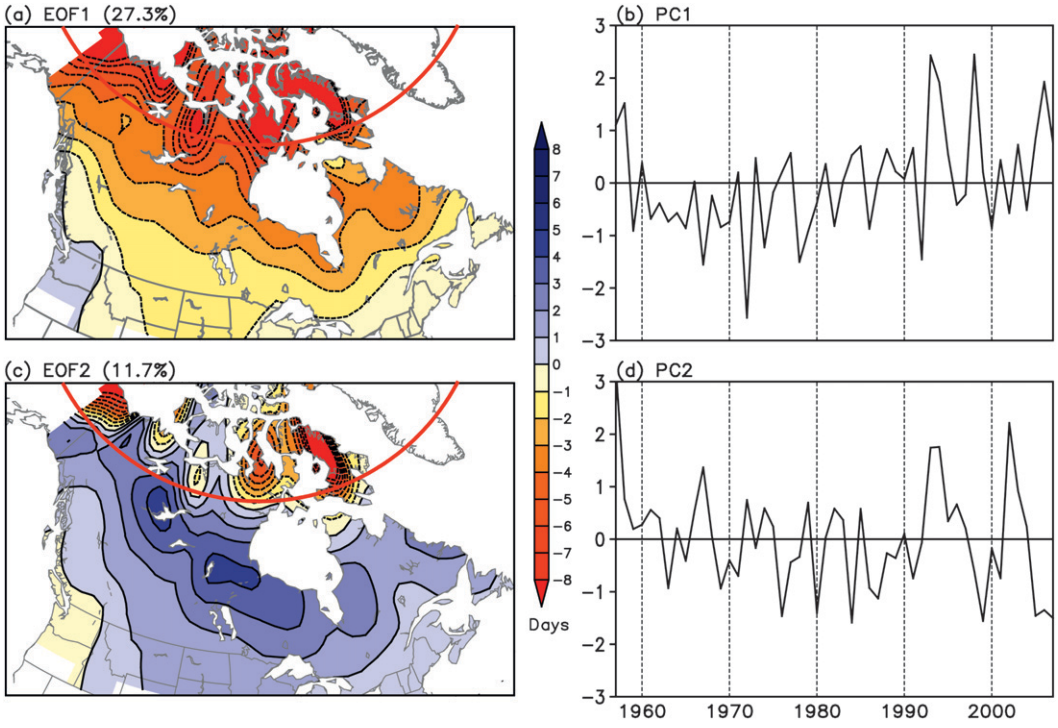

FIG. 2. (a) Spatial pattern (color shadings in days) and (b) the corresponding PC of the first EOF mode of the KFF across Canada during the cool/overwintering-crop growing season from 1957 to 2007. (c),(d) As in (a),(b), but for the second mode. The numbers in the parentheses indicate the fractional variance of the EOF modes. The red curves in (a) and (c) denote 65°N.

to time series of the KFF(DC) and KFF(IA) index along with the climatology. One evident feature in a high KFF (DC) year is an anomalous Ts cooling area prevailing over the North American (NA) continent and centered in northern Canada (color shadings in Fig. 4b). The Ts pattern in Canada well resembles the spatial pattern of the EOF1 mode if the corresponding spatial pattern reverses its sign (Fig. 2a), the correlation coefficient between KFF(DC) and PC1 reaching −0.52 [significant at greater than the 5% level based on the Student's *t* test and the effective degree of freedom calculated according to the method proposed by Chen (1982)]. This pattern indicates that more killing-frost events in Canada are often accompanied by a cooler than normal AM, and vice versa. Another pronounced feature is a dipole pattern of sea level pressure (SLP) in the eastern Pacific (contours in Fig. 4b). A notable positive SLP anomaly center occupies the North Pacific with significant anticyclonic wind anomalies at 925 hPa (vectors in Fig. 4b). This positive SLP center is located slightly to the north of the climatological Hawaiian high pressure system (Fig. 4a). Meanwhile, a negative SLP anomaly center controls the subtropical North Pacific, with cyclonic wind anomalies at 925 hPa (contours in Fig. 4b). Such flow configuration indicates a northward-shifted Hawaiian high pressure system and favors cold air from the north.

For a high KFF(IA) year (Fig. 4c), the surface circulation pattern is similar to that of a high KFF(DC), except that the positive SLP anomaly center prevailing over the North Pacific is stronger than its DC counterpart, with its high ridge expanding more eastward, toward south-central Canada (contours in Fig. 4c). A cool Ts anomaly center controls south-central Canada (south of 65°N), which overlaps with the positive KFF anomaly center of the EOF2 mode (Fig. 2c). In fact, the correlation coefficient between KFF(IA) and PC2 is 0.38, significant at greater than the 1% level based on the Student's *t* test.

Figure 5 compares AM circulation anomalies at 500 hPa regressed to the two components of the KFF index time series along with the climatology. For the DC component (Fig. 5b), the circulation pattern in the middle troposphere is similar to that near the surface. Such a barotropic structure indicates that the circulation anomalies associated with the DC component may originate from a remote forcing. According to Wu et al. (2012), the physical mechanism may be interpreted as follows. In a high KFF(DC) year, Canada is basically controlled by continental-scale middle–low-troposphere low pressure

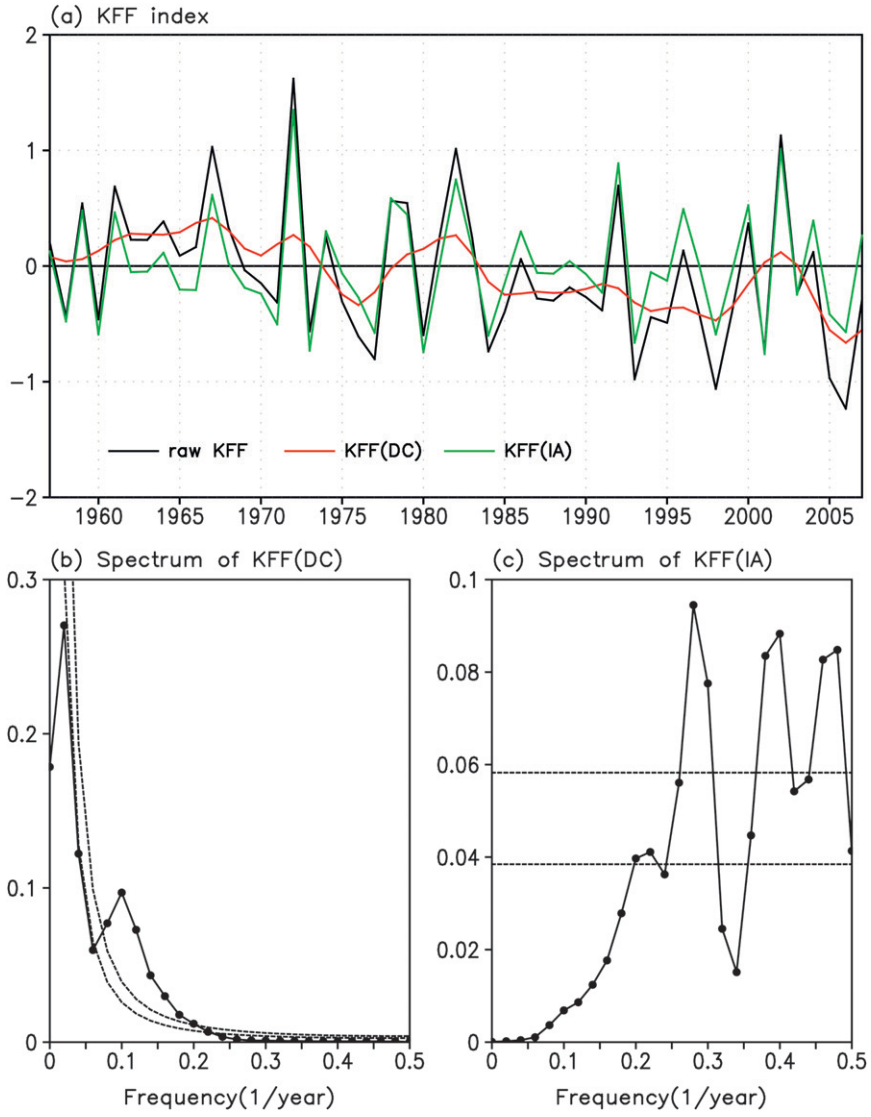

FIG. 3. (a) Time series of the standardized KFF index for 1957–2007 (black curve) and its DC (red curve) and IA (green curve) components. (b),(c) Corresponding power spectrum of the DC and IA components of the KFF index time series.

anomalies (Fig. 5b); the ascending movements associated with the low pressure anomalies cool and wet the boundary layer, enhancing cloud formation; the resulting surface radiative cooling further cools the surface. Such processes may favor the occurrence of more killing-frost events. For a low KFF(DC) AM, the situation is just the opposite.

For the IA component (Fig. 5c), the circulation anomalies at 500 hPa over south-central Canada exhibit an opposite variation tendency compared to that near the surface, namely, a baroclinic structure (Figs. 5c and 4c). In a high KFF(IA) year, the high-level jet stream tends to be intensified over the middle of NA (40°–60°N) (Figs. 5a and 5c). The strengthened baroclinic structure may increase synoptic eddy activities and consequently leads to more killing-frost events in south-central Canada. In a low KFF(IA) year, the situation is just the opposite: the high-level jet stream tends to be weakened over the middle of NA. The reduced baroclinicity may suppress synoptic eddy activities and favor less killing-frost events in south-central Canada.

To identify potential predictability sources associated with the DC and IA components of the KFF variations, we employ the PLS regression method to find the most dominant SST modes that best explain the covariations between SST and the KFF index. Figure 6 presents the four leading modes of preceding winter (DJF) SST corresponding to the KFF(DC) index from the PLS

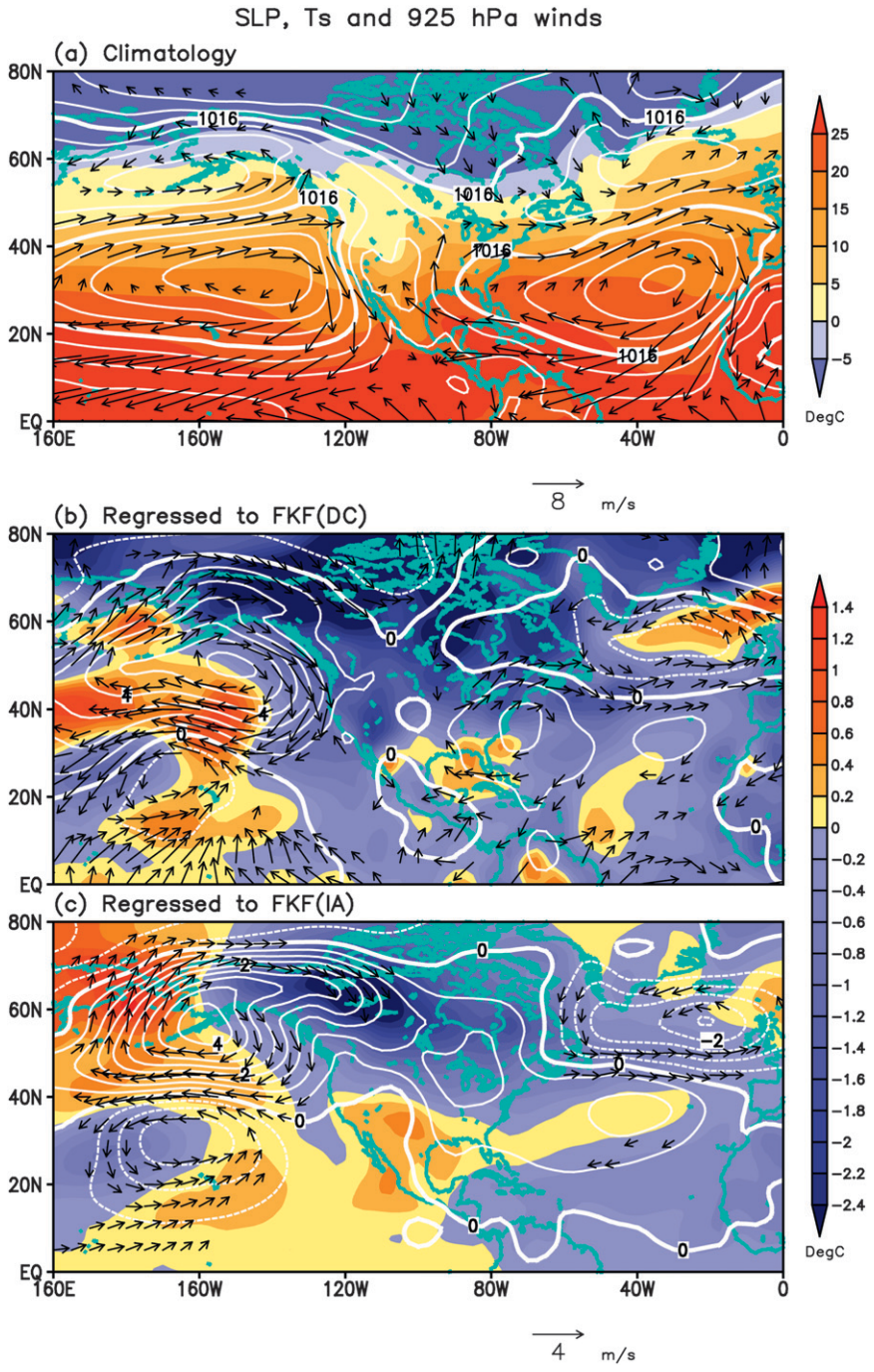

FIG. 4. The AM (a) climatology in SLP (contours in hectopascals), surface air temperature (Ts; color shadings in degrees Celsius), and 925-hPa winds (vectors in meters per second), and their anomalies regressed to the (b) KFF(DC) and (c) KFF(IA), as defined in Fig. 3. Only wind speed anomalies above 1 m s^{-1} are plotted.

regression analysis for the 41-yr period (1956–96). These modes in total account for 87.8% of the total variance of the KFF(DC) index. Note that SST data after the 1996/97 winter are not used, as we employ them for the real forecast. The significance of each mode is reflected by two numbers: the first one is the percentage of variance in the KFF(DC) index explained by the SST pattern; the other one is the percentage of total SST variance explained by the same SST pattern. Thus, in building the regression model, the PLS method searches

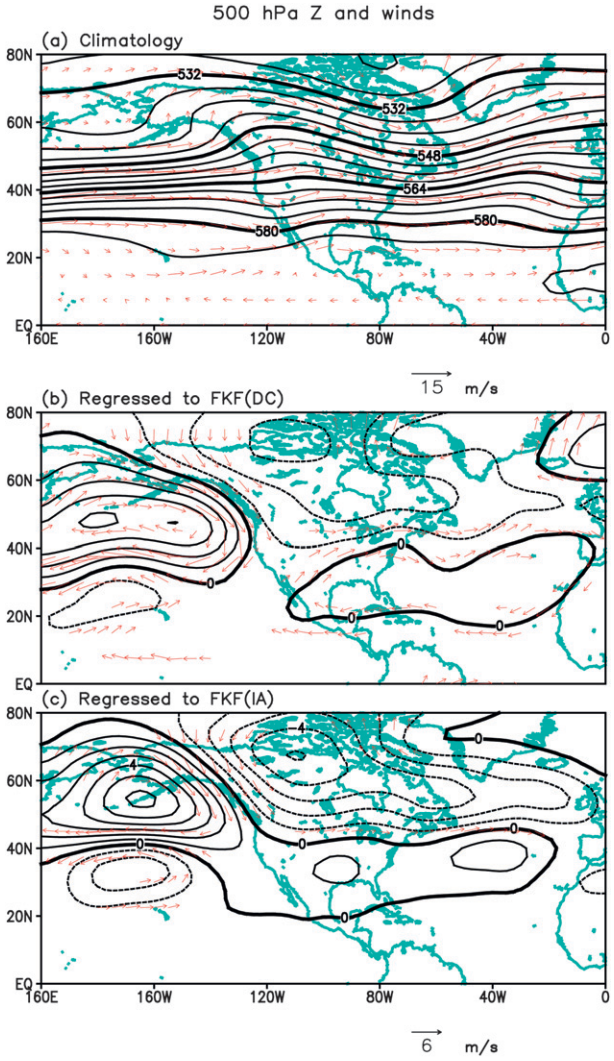

FIG. 5. As in Fig. 4, but for 500-hPa geopotential height (Z; contours in geopotential decameters) and winds (vectors; m s^{-1}). Only wind speed anomalies above 2 m s^{-1} are plotted.

for SST patterns that not only reflect the PCs of the SST variations but are also closely related to the variations in the DC component of the KFF index.

A prominent feature in Fig. 6 is that the first two leading SST modes exhibit obvious ENSO patterns (e.g., Ropelewski and Halpert 1986). Their correlation coefficients with the Niño-3.4 index reach −0.61 and 0.84, respectively (Table 1), significant at greater than the 5% level based on the Student's t test with adjusted degrees of freedom. The equatorial Pacific signal of the second SST mode occurs closer to the central Pacific than that of the first mode does (Figs. 6b and 6a). The former resembles a pattern corresponding to the central Pacific or Modoki-type ENSO (Weng et al. 2007; Yeh et al. 2009), while the latter corresponds to the traditional or eastern Pacific ENSO. In addition, the first mode also has signals in middle and high latitudes of the North Pacific and is significantly correlated with the PDO (e.g., Mantua and Hare 2002); their correlation coefficient being −0.60. The third and fourth leading modes have a weak linkage with the PDO, their correlation coefficients being −0.27 and 0.29, respectively (Table 1), which indicates that other processes besides ENSO and the PDO may also contribute to the variability of the KFF(DC).

Figure 7 displays the four leading SST modes associated with the IA component of the KFF index, which account for 65% of the total variance of the KFF(IA) index. In general, these SST modes have signals in both the tropical and mid–high-latitude North Pacific, which are similar to their DC counterparts. For instance, the first two leading modes are highly related to both ENSO and the PDO (Table 1). The third and fourth modes also bear an intimate linkage with the PDO, while the latter has a moderate correlation with ENSO in the meanwhile, their correlation coefficient being −0.30.

To summarize, ENSO and the PDO might be two dominant factors for the KFF variability in south-central Canada and these leading modes may provide potential predictability sources for the KFF variations. In the following section, we will examine their contribution to seasonal prediction of the KFF.

5. Seasonal prediction

To confirm the contribution of the above predictors to the seasonal prediction of KFF, two empirical seasonal prediction models are developed using the PLS regression method for the DC and IA components of the KFF index, respectively. We use a 41-yr training period from 1957 to 1997 to build the PLS regression models and perform a 10-yr (1998–2007) real forecast to examine their skill. Although Figs. 6 and 7 only present the first four leading modes, we found that using five leading modes for the DC component and eight leading modes for the IA component gives a better degree of forecasting skill (not shown). For comparison purposes, we also calculated the skill of the 1-month-lead hindcast from CanSIPS, which are initialized at 0000 UTC 1 March. Its calculation procedure is as follows. First, the CanSIPS hindcast data were adjusted by removing the climatology and variance differences between the observations and CanSIPS; then the hindcast KFF indices for 10-member CanCM3 and 10-member CanCM4 simulations are calculated member by member, individually; and, finally, the 20-member ensemble mean is used as the CanSIPS hindcast KFF indices.

Figure 8 presents the skill of reproduction and real-time forecasts. During the 41-yr training period (1957–97),

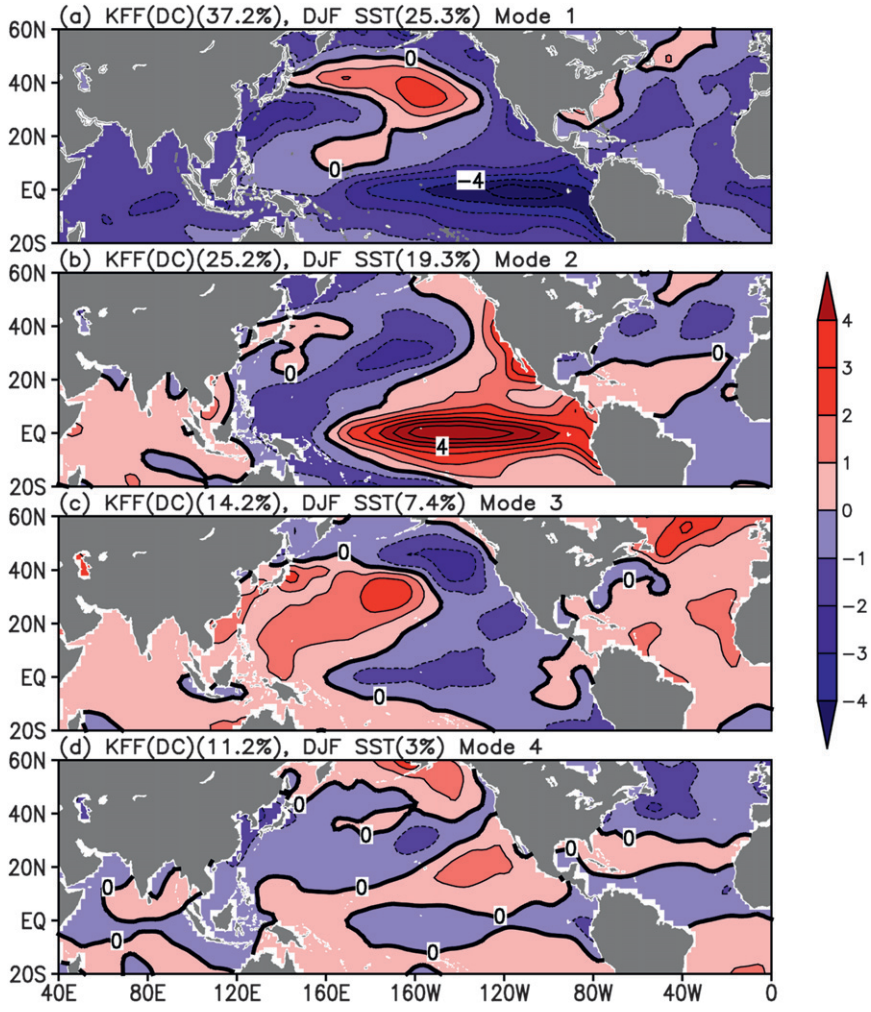

FIG. 6. (top to bottom) First four leading modes of DJF SST from PLS regression analysis for the period 1957–2007. The first percentage number is the total variance of the KFF(DC) index explained by the SST mode and the second number is the total SST variance explained by the same mode.

the PLS model can reproduce the KFF index time series with an excellent degree of skill: the correlation coefficient between the observed and the reconstructed KFF index time series reaches 0.97 and the root-mean-square error (RMSE) is 0.13. Moreover, the model exhibits a reasonable level of skill in the real forecast period of 1998–2007. The correlation coefficient between the observation (black curve) and the PLS forecast (red curve) is 0.77 and the RMSE is 0.59. For comparison purposes, we also calculated the KFF index of the CanSIPS 1-month-lead hindcast data during the same period (1998–2007) (green curve). The correlation coefficient between the observation and the CanSIPS hindcast is 0.73 and the RMSE is 0.8. Therefore, the PLS skill is comparable to or even better than the CanSIPS hindcast. Note that our PLS model uses the DJF SST data and the forecast can be made in early March. Thus, the PLS forecast is actually 1 month or even earlier before occurrences of killing-frost events, which are basically in the AM season. Therefore, this statistical

TABLE 1. Correlations between SST modes in Figs. 6 and 7 with the DJF PDO and Niño-3.4 index.

SST mode	DJF PDO	DJF ENSO
1 (DC)	−0.60	−0.61
2 (DC)	0.14	0.84
3 (DC)	−0.27	−0.08
4 (DC)	0.29	−0.07
1 (IA)	−0.68	−0.86
2 (IA)	−0.51	0.40
3 (IA)	0.51	−0.04
4 (IA)	0.52	−0.30

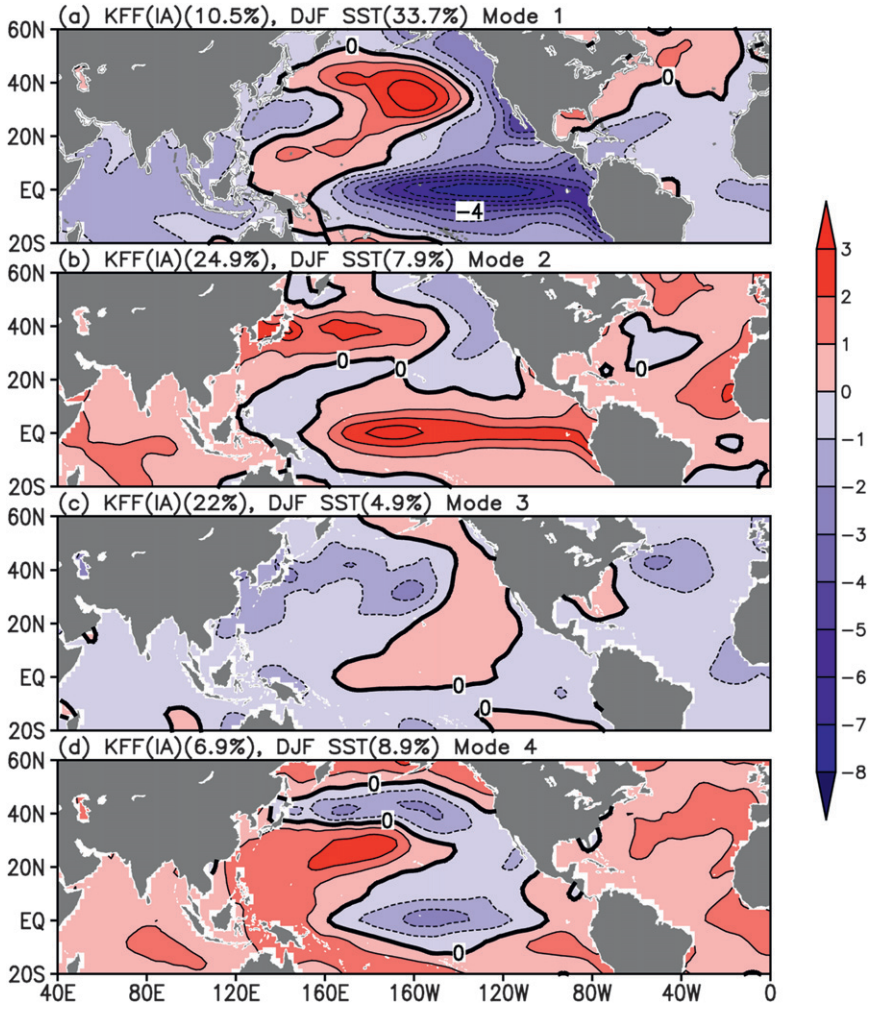

FIG. 7. As in Fig. 6, but for the KFF(IA) index.

model provides a useful prediction tool for agroclimatic events in Canada.

6. Discussion and conclusions

Studies into the seasonal prediction of agrometeorological conditions in Canada are relatively few, yet are of critical importance for the Canadian agricultural sector in identifying risks in advance. This paper focuses on seasonal prediction of the KFF during the cool/wintering-crop season in south-central Canada. Based on observational daily Ts data at 210 stations across Canada (Vincent et al. 2002), we find that most killing-frost events (86.2% of the total) occur in the AM season and exhibit a consistent variability over south-central Canada (south of 65°N). A KFF index is proposed and defined as the mean KFF of 187 temperature stations south of 65°N to quantify the KFF year-to-year variations. The variability of the KFF in south-central Canada is basically dominated by the DC and IA components, with peak periodicities around 11 and 2.5–3.8 yr, respectively. Their three-dimensional circulation structures are also examined.

To identify the predictability sources of the KFF variations, the PLS regression method is utilized to uncover the leading SST modes during the preceding DJF. These modes resemble patterns that are highly relevant to ENSO or the PDO. This indicates that ENSO and the PDO might be two dominant factors affecting the KFF variability. Based on a 41-yr training period (1957–97), a PLS seasonal prediction model is established to predict the KFF variability using the five leading SST modes associated with the DC component and the eight leading SST modes with the IA component. One-month-lead real forecasts are performed for the period 1998–2007. A promising level of prediction skill is obtained, which is comparable to or even better than that of the 1-month-lead hindcast achieved by CanSIPS. Therefore, this PLS

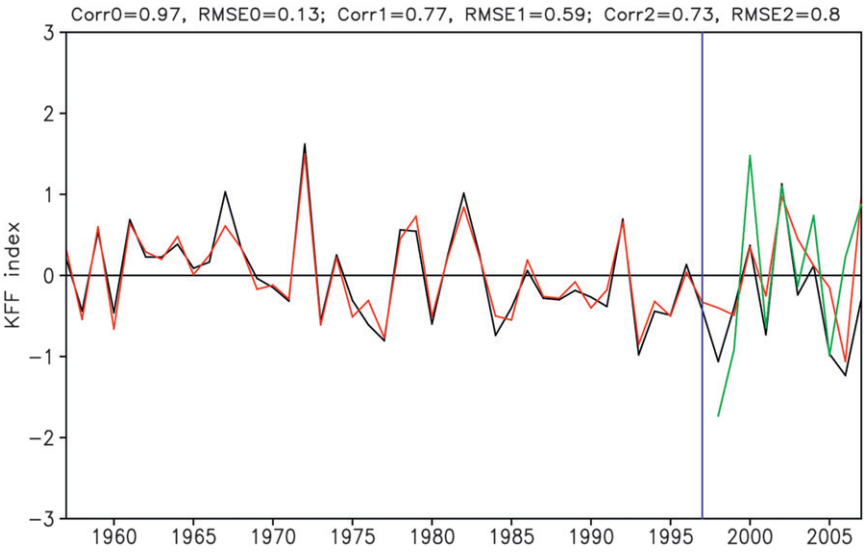

FIG. 8. PLS regression model results for forecasting the KFF index based on five SST modes corresponding to the DC component of the KFF index and eight SST modes corresponding to the IA component. The black curve is the observed KFF index. The red curve for the period 1957–97 is the reconstructed KFF index with the SST modes, and that for the period 1998–2007 is the PLS model forecast. The green curve indicates the 1-month-lead hindcast by CanSIPS. The Corr0 and RMSE0 are the correlation and RMSE between the reconstructed and observed KFF indices for the period 1957–97, Corr1 and RMSE1 are the PLS results for the forecast period 1998–2007, and Corr2 and RMSE2 are for the CanSIPS results.

model provides a useful seasonal prediction tool for agrometeorological events in Canada.

Although ENSO and the PDO are regarded as two principal predictability sources, an outstanding issue is how these patterns impact the KFF variability in south-central Canada. It has been well established that the influence of ENSO extends to North America through atmospheric teleconnections related to tropical diabatic forcing (e.g., Horel and Wallace 1981). Some studies found ENSO and the PDO influence SST, SLP, and surface wind in very similar ways and the most obvious difference between them is the time scale (Gershunov and Barnett 1998; Mantua 2001). Many studies have attempted to unveil the effect of the PDO and ENSO on each other. The results have been largely inconclusive and/or contradictory. However, Gershunov and Barnett (1998) suggested that the PDO has a modulating effect on the climate patterns resulting from ENSO. They also pointed out that this does not mean that the PDO physically controls ENSO, but rather that the resulting climate patterns interact with each other.

Although the detailed physical mechanism on how ENSO and the PDO influence the KFF variability is not yet clear, the circulation structures associated with the DC and IA components of the KFF variations may imply two possible processes. One is through a certain barotropic teleconnection, modulating the continental-scale pressure anomalies in south-central Canada, the boundary layer conditions, the local cloud formations, and in turn the occurrence of the killing-frost events. The other is through modifying the upper-level jet stream across south-central Canada, changing the local baroclinicity and, consequently, the occurrence of the killing-frost events. Nevertheless, these speculations call for further numerical and theoretical studies.

In addition to SST anomalies (SSTAs), snow cover or other low boundary anomalies may also contribute to the KFF variability. For instance, Wu et al. (2011b) and Lin and Wu (2011, 2012) revealed the potential effects of snow cover on seasonal mean surface temperature conditions over North America. However, because of the limitation of the PLS method, we did not analyze the role of snow cover in this work and may do a further investigation in the future.

Acknowledgments. Zhiwei Wu is supported by the Sustainable Agriculture Environment Systems (SAGES) research initiative of Agriculture and Afri-Food Canada through the Natural Sciences and Engineering Research Council of Canada (NSERC) Fellowship Program, the National Basic Research Program ''973'' (Grant 2013CB430202), and a project funded by the Priority Academic Program Development of Jiangsu Higher Education Institutions (PAPD). Yun Li is supported by the Indian Ocean Climate Initiative. We thank three anonymous reviews for their constructive comments.

REFERENCES

Arora, V., and Coauthors, 2011: Carbon emission limits required to satisfy future representative concentration pathways of greenhouse gases. *Geophys. Res. Lett.,* **38,** L05805, doi:10.1029/2010GL046270.

Barnett, T. P., L. Dümenil, U. Schlese, E. Roeckner, and M. Latif, 1987: The effect of Eurasian snow cover on global climate. *Science,* **239,** 504–507.

Charney, J. G., and J. Shukla, 1981: Predictability of monsoons. *Monsoon Dynamics,* J. Lighthill and R. P. Pearce, Eds., Cambridge University Press, 99–109.

Chen, W. Y., 1982: Fluctuations in Northern Hemisphere 700 mb height field associated with Southern Oscillation. *Mon. Wea. Rev.,* **110,** 808–803.

Dee, D. P., and Coauthors, 2011: The ERA-Interim reanalysis: Configuration and performance of the data assimilation system. *Quart. J. Roy. Meteor. Soc.,* **137,** 553–597.

Flato, G. M., and W. D. I. Hibler, 1992: Modelling pack ice as a cavitating fluid. *J. Phys. Oceanogr.,* **22,** 626–651.

Gershunov, A., and T. P. Barnett, 1998: Interdecadal modulation of ENSO teleconnections. *Bull. Amer. Meteor. Soc.,* **79,** 2715–2725.

Haenlein, M., and A. Kaplan, 2004: A beginner's guide to partial least squares analysis. *Understanding Stat.,* **3,** 283–297.

Horel, J. D., and J. M. Wallace, 1981: Planetary-scale atmospheric phenomena associated with the Southern Oscillation. *Mon. Wea. Rev.,* **109,** 813–829.

Lee, W., and B. Merryfield, 2010: The Second Coupled Historical Forecasting Project (CHFP2). *Proc. 44th Annual Congress of the Canadian Meteorological and Oceanographic Society–36th Annual Scientific Meeting of the Canadian Geophysical Union,* Ottawa, ON, Canada, CMOS–CGU.

Lin, H., and Z. Wu, 2011: Contribution of the autumn Tibetan Plateau snow cover to seasonal prediction of North American winter temperature. *J. Climate,* **24,** 2801–2813.

——, and ——, 2012: Contribution of Tibetan Plateau snow cover to the extreme winter condition of 2009–2010. *Atmos.–Ocean,* **50,** 86–94.

Lorenz, E. N., 1965: A study of the predictability of a 28-variable model. *Tellus,* **17,** 321–333.

Mantua, N. J., 2001: The Pacific decadal oscillation. *The Earth System: Physical and Chemical Dimension of Global Environmental Change,* M. C. McCracken and J. S. Perry, Eds., *Encyclopedia of Global Environmental Change,* Vol. 1, Wiley, 592–594.

——, and S. R. Hare, 2002: The Pacific decadal oscillation. *J. Oceanogr.,* **58,** 35–44.

Namias, J., 1959: Recent seasonal interaction between North Pacific waters and the overlying atmospheric circulation. *J. Geophys. Res.,* **64,** 631–646.

——, 1965: Macroscopic association between monthly mean sea-surface temperature and overlying winds. *J. Geophys. Res.,* **70,** 2307–2318.

North, G. R., T. L. Bell, R. F. Cahalan, and F. J. Moeng, 1982: Sampling errors in the estimation of empirical orthogonal functions. *Mon. Wea. Rev.,* **110,** 699–706.

Qian, B., X. Zhang, K. Chen, Y. Feng, and T. O'Brien, 2010: Observed long-term trends for agroclimatic conditions in Canada. *J. Appl. Meteor. Climatol.,* **49,** 604–618.

Robinson, D. A., K. F. Dewey, and R. R. Heim, 1993: Global snow cover monitoring: An update. *Bull. Amer. Meteor. Soc.,* **74,** 1689–1696.

Ropelewski, C. F., and M. S. Halpert, 1986: North American precipitation and temperature patterns associated with the El Niño/Southern Oscillation (ENSO). *Mon. Wea. Rev.,* **114,** 2352–2362.

Scinocca, J. F., N. A. McFarlane, M. Lazare, and J. Li, 2008: The CCCma third generation AGCM and its extension into the middle atmosphere. *Atmos. Chem. Phys.,* **8,** 7055–7074.

Shabbar, A., and M. Khandekar, 1996: The impact of El Niño–Southern Oscillation on the temperature field over Canada. *Atmos.–Ocean,* **34,** 401–416.

——, and B. Bonsal, 2003: An assessment of changes in winter cold and warm spells over Canada. *Nat. Hazards,* **29,** 173–188.

Shukla, J., 1998: Predictability in the midst of chaos: A scientific basis for climate forecasting. *Science,* **282,** 728–731.

Smith, T. M., and R. W. Reynolds, 2004: Improved extended reconstruction of SST (1854–1997). *J. Climate,* **17,** 2466–2477.

Smoliak, B. V., J. M. Wallace, M. T. Stoelinga, and T. P. Mitchell, 2010: Application of partial least squares regression to the diagnosis of year-to-year variations in Pacific Northwest snowpack and Atlantic hurricanes. *J. Geophys. Res.,* **37,** L03801, doi:10.1029/2009GL041478.

Uppala, S. M., and Coauthors, 2005: The ERA-40 Re-Analysis. *Quart. J. Roy. Meteor. Soc.,* **131,** 2961–3012, doi:10.1256/qj.04.176.

Verseghy, D., 2008: CLASS—The Canadian Land Surface Scheme (version 3.4). Tech. Doc. Version 1.1, Climate Research Branch, Science and Technology Division, Environment Canada, 178 pp.

Vincent, L. A., and E. Mekis, 2006: Changes in daily and extreme temperature and precipitation indices for Canada over the twentieth century. *Atmos.–Ocean,* **44,** 177–193.

——, X. Zhang, B. R. Bonsal, and W. D. Hogg, 2002: Homogenization of daily temperatures over Canada. *J. Climate,* **15,** 1322–1334.

Wang, B., R. Wu, and X. Fu, 2000: Pacific–East Asia teleconnection: How does ENSO affect East Asian climate? *J. Climate,* **13,** 1517–1536.

——, Z. Wu, J. Liu, C.-P. Chang, J. Li, and T.-J. Zhou, 2010: Another look at climate variations of the East Asian winter monsoon: Northern and southern modes. *J. Climate,* **23,** 1495–1512.

Weng, H., K. Ashok, S. Behera, S. Rao, and T. Yamagata, 2007: Impacts of recent El Niño Modoki dry/wet conditions in the Pacific rim during boreal summer. *Climate Dyn.,* **29,** 113–129.

Wu, Z., B. Wang, J. Li, and F.-F. Jin, 2009: An empirical seasonal prediction model of the East Asian summer monsoon using ENSO and NAO. *J. Geophys. Res.,* **114,** D18120, doi:10.1029/2009JD011733.

——, J. Li, Z. Jiang, and J. He, 2011a: Predictable climate dynamics of abnormal East Asian winter monsoon: Once-in-a-century snowstorms in 2007/2008 winter. *Climate Dyn.,* **37,** 1661–1669.

——, H. Lin, and T. Brien, 2011b: Seasonal prediction of air temperature associated with the growing season start of warm-season crops across Canada. *J. Appl. Meteor. Climatol.,* **50,** 1637–1649.

——, ——, J. Li, Z. Jiang, and T. Ma, 2012: Heat wave frequency variability over North America: Two distinct leading modes. *J. Geophys. Res.,* **117,** D02102, doi:10.1029/2011JD016908.

Yeh, S. W., J. S. Kug, B. Dewitte, M. H. Kwon, B. P. Kirtman, and F. F. Jin, 2009: El Niño in a changing climate. *Nature,* **461,** 511–514.

Zhang, H., J. Qin, and Y. Li, 2011: Climatic background of cold and wet winter in southern China: Part 1. Observational analysis. *Climate Dyn.,* **37,** 2335–2354.

Zhang, X., L. A. Vincent, W. D. Hogg, and A. Niitsoo, 2000: Temperature and precipitation trends in Canada during the 20th century. *Atmos.–Ocean,* **38,** 395–429.